Fuzzy Geodesics and Consistent Sparse Correspondences For Deformable Shapes

Jian Sun and Xiaobai Chen and Thomas A. Funkhouser

Princeton University, Princeton NJ, 08544 USA

Abstract

A geodesic is a parameterized curve on a Riemannian manifold governed by a second order partial differential equation. Geodesics are notoriously unstable: small perturbations of the underlying manifold may lead to dramatic changes of the course of a geodesic. Such instability makes it difficult to use geodesics in many applications, in particular in the world of discrete geometry. In this paper, we consider a geodesic as the indicator function of the set of the points on the geodesic. From this perspective, we present a new concept called fuzzy geodesics *and show that fuzzy geodesics are stable with respect to the Gromov-Hausdorff distance. Based on fuzzy geodesics, we propose a new object called* the intersection configuration *for a set of points on a shape and demonstrate its effectiveness in the application of finding consistent correspondences between sparse sets of points on shapes differing by extreme deformations.*

Categories and Subject Descriptors (according to ACM CCS):   I.3.3 [Computer Graphics]: Picture/Image Generation—Line and curve generation

1. Introduction

The shortest geodesic between two points on a complete Riemannian manifold is the path whose length is shortest. This path conveys much richer information about the underlying manifold than the geodesic distance itself. However, there may exist multiple shortest geodesics between two points on a manifold, which makes the shortest geodesic notoriously unstable. Small perturbations of the underlying manifold may lead to a dramatic change of the shortest geodesic, and thus it is difficult to use geodesics in shape analysis applications.

To overcome this limitation, we propose a new concept called *fuzzy geodesics*. The fuzzy geodesic for any two points p and q is a function over the underlying manifold indicating for every point x how long is the shortest path from p to q through x in comparison to the shortest geodesic from p to q directly. The main value of this formulation is that it provides a stable way to utilize geodesics in shape analysis applications. We prove that fuzzy geodesics are stable with respect to perturbations as measured by the Gromov-Hausdorff distance (Section 3).
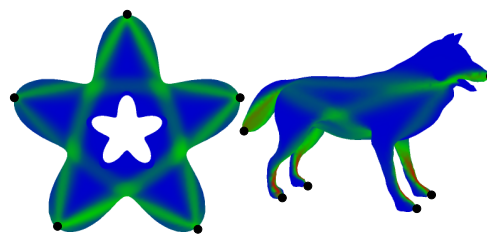
Figure 1: *The sum of the fuzzy geodesics between all pairs of marked points.*

Comparing to the geodesic distance which by definition is stable with respect to the Gromov-Hausdorff distance, fuzzy geodesics encode much richer geometric information. In many applications, a set of feature points is often used to represent a shape, where the spatial relationship between these feature points is important, but difficult to express. With the help of fuzzy geodesics which act like a set of fuzzy ropes bounding the shape (Figure 1), we introduce a new way to describe the spatial arrangement of a set of

points on a manifold using the intersection pattern of pairwise fuzzy geodesics, which we call *intersection configuration*(Section 4). We find that differences in this *intersection configuration* are effective at distinguishing correct point correspondences from incorrect ones during experiments with a variety of meshes differing by extreme deformations (Section 5).

2. Background and related work

A geodesic on a Riemmannian manifold M is a curve γ : $I \rightarrow M$ such that the changing rate of the tangent vector of γ (given by the covariant derivative) vanishes at any point on γ. The geodesic is a classical concept in differential geometry and has been studied extensively [dC92]. The geodesic distance between any two points $p, q \in M$, denoted as $d_M(x, y)$, is the infimum of the lengths of all path joining p, q. If the manifold M is complete, there must exist a minimizing geodesic joining p, q that attains the geodesic distance, which we will call the geodesic between p, q for the remainder of the paper.

In the discrete setting, computing the geodesics has been studied extensively [Pap85]. Mitchell et al. [MMP87] presented an algorithm to compute the shortest geodesic between any two points on a polygonal surface, and Surazhsky et al. proposed a fast implementation [SSK*05]. Dijkstra's algorithm can also be used to find approximate geodesics by working with a graph formed by the mesh's 1-skeleton.

The convergence of geodesics has also been studied [HPW06, DL09], where a discrete representation (e.g., polygonal surface or point set) is considered as an approximation of some smooth manifold. The convergence of geodesics studies if a shortest path on the discrete representation converge to a geodesic on the smooth manifold when the approximation error of the discrete representation to the smooth manifold goes to zero. Hildebrandt et al [HPW06] and Dey and Li [DL09] show the subsequence convergence of geodesics from polygonal surfaces and point clouds respectively.

However, the convergence of geodesics does not imply it is stable. In particular, geodesics are not stable at cut points. A cut point of a geodesic γ issued from the point p is the point where γ ceases to be minimizing. The cut locus of p is all cut points on the geodesics issued from p. If there are multiple geodesics between p, q, then p is on the *cut locus* of q and vice verse. Therefore, if a geodesic passing through two points that are close to each other's cut locus, small perturbations may lead to dramatic change of that geodesic.

3. Fuzzy Geodesics

In this section, we define fuzzy geodesics, and show their stability with respect to perturbations.

Definition: To define fuzzy geodesics, let us consider the image of the geodesic γ on the manifold M, also denoted as γ. The indicator function of γ, denoted as χ_γ, is defined as follows: $\chi_\gamma(x) = 1$ if $x \in \gamma$ and 0 otherwise. The indicator function χ_γ is an equivalent representation of γ. The idea of fuzzy geodesic is basically to obtain a smoothed indicator function. However, naively smoothing the indicator function will not make it stable due to the existence of multiple minimizing geodesics between two points. To overcome this problem, we introduce the fuzzy geodesic, which is defined as follows.

Definition 3.1 *Given a parameter $\sigma > 0$, the fuzzy geodesic between any two points p and q on a Riemannian manifold M is defined as a function $\mathcal{G}_{p,q}^{\sigma} : M \rightarrow \mathbb{R}$:*

$$\mathcal{G}_{p,q}^{\sigma}(x) = \exp\left(-\frac{|d_M(x,p) + d_M(x,q) - d_M(p,q)|}{\sigma}\right). \quad (1)$$

Intuitively, the fuzzy geodesic $\mathcal{G}_{p,q}^{\sigma}(x)$ indicates for every point x how long is the shortest path from p to q through x in comparison to the shortest geodesic from p to q directly. It attains the maximum value of one at points on the shortest geodesic(s) between p and q and less values (between zero and one) at other points (Figure 2). If there are multiple shortest geodesics, $\mathcal{G}_{p,q}^{\sigma}(x)$ reaches maximum on all of them.

The parameter σ controls the fuzziness. The bigger the σ is, the fuzzier fuzzy geodesics are. In the extreme, when σ goes to infinity, $\mathcal{G}_{p,q}^{\sigma}$ becomes a constant function 1. When σ goes to 0, $\mathcal{G}_{p,q}^{\sigma}(x)$ becomes the indicator function of all minimizing geodesics between p, q. In between, larger values of σ produce fuzzy geodesics with larger values at points further from the shortest geodesic (Figure 2).

The time complexity of computing the fuzzy geodesic between two points is the same as that of computing the geodesic distance from two sources to all other points. In particular, on a triangle mesh with n vertices, if we use Dijkstra's algorithm to approximate geodesic distance over the 1-skeleton of the mesh, the complexity of computing fuzzy geodesic between a pair of points is $O(n \log n)$.

It should be noted that the fuzzy geodesics definition is very general (it depends only on a distance metric), and thus fuzzy geodesics can be computed for a wide variety of input types, including meshes, point clouds, graphs, etc., as long as a distance between points can be defined.

Stability: To analyze the stability of fuzzy geodesics, we consider how the fuzzy geodesic function changes in relation to the Gromov-Hausdorff distance as a shape deforms [Gro99]. The Gromov-Hausdorff distance is commonly used to measure shape deformations [MS05,SMC07], and thus it provides a good measure for how similar two shapes are. Our goal is to show that two shapes with a small Gromov-Hausdorff distance provably have a small difference in their fuzzy geodesics.
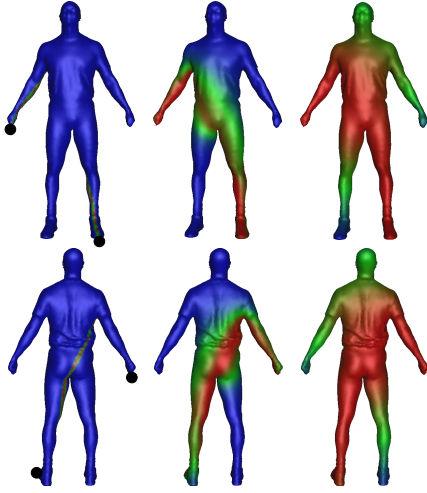
Figure 2: *Fuzzy geodesics between two fixed points with the parameter σ equals 0.05%, 5%, 500% of the geodesic diameter respectively from left to right. Both front (top) and back (bottom) are shown.*

Formally, the Gromov-Hausdorff distance between two metric spaces (X, d_X) and (Y, d_Y), denoted $d_{GH}(X, Y)$, is defined as

$$d_{GH}(X, Y) = \inf_{Z, f, g} d_H^Z(f(X), g(Y)) \quad (2)$$

where $f : X \rightarrow Z$ and $g : Y \rightarrow Z$ are isometric embeddings into the metric space Z and d_H^Z is the Hausdorff distance in the space Z. Note that the usual embedding of a surface into $\mathbb{R}^3$ by inclusion is often not isometric as the geodesic distance between two points on the surface is different from their Euclidean distance in $\mathbb{R}^3$. Nevertheless, such a space Z does always exist. For example, the product of X and Y with the metric $d_X + d_Y$ is a possible choice of Z.

If X, Y are bounded, then we have the following equivalent definition, see [MS05] and the references therein.

$$d_{GH}(X, Y) = \inf_{f, g} \max\{A(f), B(g), C(f, g)\} \quad (3)$$

where $f : X \rightarrow Y$ and $g : Y \rightarrow X$ are any function and

$$A(f) = \sup_{x_1, x_2 \in X} |d_X(x_1, x_2) - d_Y(f(x_1), f(x_2))| \text{ and}$$
$$B(f) = \sup_{y_1, y_2 \in Y} |d_Y(y_1, y_2) - d_X(g(y_1), g(y_2))| \text{ and}$$
$$C(f, g) = \sup_{x \in X, y \in Y} |d_X(x, g(y)) - d_Y(f(x), y)|. \quad (4)$$

As the definition of fuzzy geodesics only involves the distances, the stability of fuzzy geodesics follows from the definition of the Gromov-Hausdorff distance in a straightforward way. For the same reason, fuzzy geodesics can be extended and defined on any metric space and thus we state our stability theorem in this more general setting.
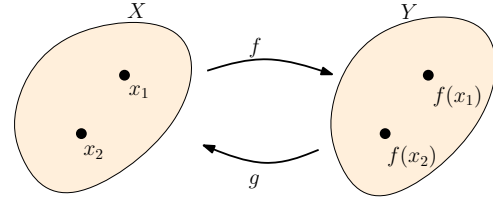
Figure 3: *Illustration of Theorem 3.2.*

Theorem 3.2 *For any two bounded metric spaces (X, d_X) and (Y, d_Y), there exist the maps $f : X \rightarrow Y$ and $g : Y \rightarrow X$ such that*

1. *for any two points $x_1, x_2 \in X$,*

$$\|\mathcal{G}_{x1,x2}^{\sigma} - \mathcal{G}_{f(x_1), f(x_2)}^{\sigma} \circ f\|_{\infty} \leq \frac{4 d_{GH}(X, Y)}{\sigma} \text{ and}$$
$$\|\mathcal{G}_{x1,x2}^{\sigma} \circ g - \mathcal{G}_{f(x_1), f(x_2)}^{\sigma}\|_{\infty} \leq \frac{4 d_{GH}(X, Y)}{\sigma}.$$

2. *for any two points $y_1, y_2 \in Y$,*

$$\|\mathcal{G}_{y1,y2}^{\sigma} \circ f - \mathcal{G}_{g(y_1), g(y_2)}^{\sigma}\|_{\infty} \leq \frac{4 d_{GH}(X, Y)}{\sigma} \text{ and}$$
$$\|\mathcal{G}_{y1,y2}^{\sigma} - \mathcal{G}_{g(y_1), g(y_2)}^{\sigma} \circ g\|_{\infty} \leq \frac{4 d_{GH}(X, Y)}{\sigma}.$$

Before proving it, some explanation of this theorem is in order. Although the theorem holds for any two metric spaces, to understand the theorem, one can think of Y as a small perturbation of X, see Figure 3. The map f, g are the maps that almost retain the Gromov-Hausdorff distance, see Eqn(3). When perturbation is small, f, g give the correspondence between X and its perturbed version Y. Now let us consider the first two inequalities in the theorem. For any two points x_1, x_2 on X, we want to see how much the fuzzy geodesic $\mathcal{G}_{x_1, x_2}$ changes after perturbation. Since $f(x_1), f(x_2)$ are the corresponding points of x_1, x_2 after perturbation, it is natural to compare $\mathcal{G}_{x_1, x_2}$ with $\mathcal{G}_{f(x_1), f(x_2)}$. We can compare them over the space X (given by the first inequality), or over the perturbed space Y (given by the second inequality). The last two inequalities in the theorem can be explained in a similar way.

Proof We first prove the first inequality. Set $\varepsilon = d_{GH}(X, Y)$. If $\varepsilon = 0$, then X and Y are isometric to each other. Let f be an isometric map from X to Y and g be its inverse. Obviously, the inequality holds in this case. Now assume $\varepsilon > 0$. From Eqn(3), for any $\eta > 0$, there exist the maps $f : X \rightarrow Y$ and $g : Y \rightarrow X$ such that for any $y \in Y$, we have

$$|d_X(x_1, x_2) - d_Y(f(x_1), f(x_2))| < \varepsilon + \eta \text{ and}$$
$$|d_X(g(y), x_1) - d_Y(y, f(x_1))| < \varepsilon + \eta \text{ and}$$
$$|d_X(g(y), x_2) - d_Y(y, f(x_2))| < \varepsilon + \eta.$$

Note that both $\mathcal{G}_{x1,x2}^{\sigma} \circ g$ and $\mathcal{G}_{f(x_1), f(x_2)}^{\sigma}$ are the functions
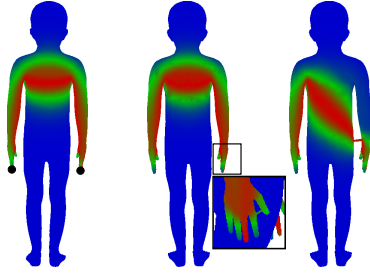
Figure 4: *Changes of fuzzy geodesics due to the change of topology.*

over Y. For any point $y \in Y$ we have

$$\begin{aligned} & | \quad (d_X(g(y),x_1)+d_X(g(y),x_2))-d_X(x1,x2)) \\ & - \quad (d_Y(y,f(x_1))+d_Y(y,f(x_2))-d_Y(f(x_1),f(x_2)))| \\ & < \quad 3(\varepsilon+\eta) \end{aligned}$$

Hence

$$|\mathcal{G}^{\sigma}_{x1,x2}(g(y))-\mathcal{G}^{\sigma}_{f(x_1),f(x_2)}(y)| < |1-e^{-\frac{3(\varepsilon+\eta)}{\sigma}}| < \frac{3(\varepsilon+\eta)}{\sigma} (5)$$

which shows the first inequality by choosing $\eta = \varepsilon/3$. The other inequalities can be proved in a similar way. Note that the map f,g can be chosen so that all four inequalities hold for fixed f,g. $\square$

The Lipschitz constant is proportional to the reciprocal of the parameter σ. This means σ controls the stability of the fuzzy geodesics. Small σ makes fuzzy geodesics less stable but more precise while big σ makes fuzzy geodesics more stable but less precise. When the Gromov-Hausdorff distance between X,Y is small, we can afford to use small σ to obtain both stable and precise fuzzy geodesics. However, when the Gromov-Hausdorff distance between X,Y are big, we have to use big σ to have stable fuzzy geodesics. Consequently fuzzy geodesics are becoming less precise.

It is interesting to see the stability of Fuzzy geodesics under topological changes. As seen from Figure 4, when the topological changes are local (e.g. middle picture in Figure 4), it does not change Fuzzy geodesics very much, while those that short cut the different parts of the shape (e.g. right picture in Figure 4) can change Fuzzy geodesics a lot, which is predicted by the stability theorem as it changes the Gromov-Hausdorff distance a lot. One way to make it stable against those changes is to define fuzzy geodesics based on diffusion distances, which we leave as future work.

In what follows, to simplify the notation, when there is no confusion, we will drop the parameter σ in our notations. For example. $\mathcal{G}_{p,q}$ denote the fuzzy geodesic between p,q for some fixed σ.

4. Intersection Configuration

In this section, we introduce a model for structural differences between point sets based on fuzzy geodesics. Intuitively, we note that the pairwise fuzzy geodesics within a set of potential point correspondences form a set of "fuzzy ropes" bounding the shape (Figure 1), and the crossing pattern of those "ropes" is indicative of the structural arrangement of the points. Therefore, we aim to represent a shape by the pattern of fuzzy geodesic intersections, which we call its *intersection configuration*.

Before defining the intersection configuration, we first define the intersection of two fuzzy geodesics, which is also a function.

Definition 4.1 *For any two pairs (p,q) and (u,v) on a Riemannian manifold M, the* intersection *of the fuzzy geodesics $\mathcal{G}_{p,q}$ and $\mathcal{G}_{u,v}$, denoted $\mathcal{I}^{u,v}_{p,q}$, is their point-wise multiplication, namely $\mathcal{I}^{u,v}_{p,q} : M \to \mathbb{R}$:*

$$\mathcal{I}^{u,v}_{p,q}(x) = \mathcal{G}_{p,q}(x) \cdot \mathcal{G}_{u,v}(x). \qquad (6)$$

It is obvious that the intersection of two fuzzy geodesics is also stable with respect to the Gromov-Hausdorff distance, but the error becomes quadratic in terms of the Gromov-Hausdorff distance. The p-norm $\|\mathcal{I}^{u,v}_{p,q}\|_p$ of the intersection function tells how much two fuzzy geodesics intersect, which is a stable isometric invariant. In particular, for small σ, $\|\mathcal{I}^{q,q}_{q,q}\|_p$ with $1 \le p < \infty$ contains the information of Gauss curvature around q as the geodesic disk of a fixed radius has big area if the Gauss curvature is negative and small area if it is positive.

Now we are ready to introduce our intersection configuration, which basically records how much each pair of fuzzy geodesics intersects.

Definition 4.2 *Given a set of points $S = \{s_i\}^m_{i=1}$ in X, its intersection configuration, denoted $\mathcal{IC}_S$, is a four dimensional square matrix of size m where the entry (i,j,k,l) is the p-norm of the intersection of the fuzzy geodesics $\mathcal{G}_{s_i,s_j}$ and $\mathcal{G}_{s_k,s_l}$, namely $\mathcal{IC}_S(i,j,k,l) = \|\mathcal{I}^{s_k,s_l}_{s_i,s_j}\|_p$.*

For a set of m points, the complexity of intersection configuration is $O(m^4)$. Note the matrix $\mathcal{IC}_S$ has three fold symmetry as $\mathcal{IC}_S(i,j,k,l) = \mathcal{IC}_S(j,i,k,l)$, $\mathcal{IC}_S(i,j,k,l) = \mathcal{IC}_S(i,j,l,k)$ and $\mathcal{IC}_S(i,j,k,l) = \mathcal{IC}_S(k,l,i,j)$. For a triangle mesh with n vertices, the complexity of computing all pairwise fuzzy geodesics is $O(mn\log n + m^2 n)$ and thus the total complexity of computing the intersection configuration of S is $O(mn\log n + m^4 n)$, if we use Dijsktra algorithm to approximate geodesic distances.

Finally, we propose a new way to determine the compatibility of a set of point correspondence based on intersection configuration, which we call *intersection configuration distance*. Specifically, given a correspondence from X to Y,

namely a set of points $S \in X$ and a map $h : S \to Y$, we want to measure how good the map h is. The intersection configuration distance evaluates the map h as the difference between $\mathcal{IC}_S$ and $\mathcal{IC}_{h(S)}$ with the proper labeling reflecting the map h. Formally,

Definition 4.3 *Given a sparse correspondence $h : S = \{s_i\}_{i=1}^m \to Y$ from X to Y, we define the intersection configuration distance as*

$$ICD(h) =$$
$$\sum_{i,j,k,l} |\mathcal{IC}_S(s_i,s_j,s_k,s_l) - \mathcal{IC}_{h(S)}(h(s_i),h(s_j),h(s_k),h(s_l))|$$

where we abuse the notation and denote $\mathcal{IC}_S(s_i,s_j,s_k,s_l)$ the entry in $\mathcal{IC}_S$ corresponding to the pairs $(s_i,s_j),(s_k,s_l)$.

The intersection configuration distance measures how similar crossings of fuzzy geodesics are, and thus we expect it is low for corresponding point set within the same semantic class, and high for other

5. Experiment: Finding Sparse Correspondences

In this section, we investigate how intersection configurations, in particular intersection configuration distances, can be useful for detecting consistent correspondences between sets of points on two shapes differing by a non-rigid deformation. This application is extremely important, as finding correspondences is at the core of many shape analysis applications [vKZHCO10]. A common approach is to enumerate sets of candidate point correspondences and then choose the sets that minimize an error function measuring dissimilarities in the spatial configurations of corresponding points. The challenge is to define a discriminating and stable error function. Several error functions have been proposed [BBK06, BR07, ZSCO*08, JZvK07, OSG08, WGQ08, LF09], most of which are aimed at measuring deviations from a particular transformation space – e.g., isometries. Thus, they are suitable for applications where those types of deformations are expected (e.g., tracking of time-varying cloth surfaces). However, they are often not adequate for modeling intra-class differences between shapes, where shape variations retain the same structure (same parts in the same arrangement), but are not well-described by a single transformation (e.g., a giraffe versus an antelope). Other methods have measured differences in skeletal graph structures [HSKK01, ATCO*10]. However, they are generally not stable – i.e., the skeletal graphs extracted for two objects of the same class may not have the same topology, which complicates the comparison of these skeletal graph structures.

Our approach is to measure differences between candidate correspondences using the *intersection configuration distance* (ICD) described in the previous section. We hypothesize that this approach will be effective, since the ICD

Model	n	m	FP (s)	IC (s)
Human	10.1	5.0	15.1	2.3
Hand	8.0	6.0	14.1	3.3
Ant	7.5	9.0	10.3	2.7
Octopus	8.8	8.0	13.6	3.5
Armadillo	21.1	18.6	33.8	19.0

Table 1: *Average complexity and timing statistics (averaged per category). **n**: number of vertices in thousands of a model; **m**: number of feature points; **FP**: time in seconds to compute HKS function and extract feature points; **IC**: time in seconds to compute intersection configuration;*

is both stable and descriptive of structural arrangements of points. The remainder of this section, describes experiments to test this hypothesis.

Data set: Our test meshes were chosen from the Watertight Models Track of SHREC 2007 Benchmark [GBP07] (Watertight in short). We test every pair of meshes within the following categories: Human, Ant, Octopus, Hand, Armadillo and Fourleg (these classes were chosen because they contain deformable shapes). The meshes were used directly without any preprocessing, such as smoothing or simplification .

Point feature detection: For each mesh in the data set, we extract a sparse set of feature points from the surface. While many methods are possible for this step, we provide one that chooses points from the maxima of a function which is invariant under isometry (with the goal of finding points likely to correspond within the same object class). The function we use is the heat kernel signature (HKS) proposed by Sun et. al [SOG09] at one large time scale (as we are looking for global correspondences). This function can be computed efficiently (empirically linear in the number of vertices in the mesh) as only a few eigenfunctions are needed to estimate HKS for a large time scale. In addition, we use persistent homology to measure the persistence of each maximum [ELZ00] where the filtration is induced by the HKS function, and then sort all the maxima in the decreasing order of their persistence. To avoid noisy maxima, we choose the first m most persistent maxima as our sparse point set.

Intersection configuration computation: For each mesh in the data set, we compute the intersection configuration of the extracted m point features. In these computations, we fixed the parameter σ to be 10% of the geodesic diameter which is evaluated as the maximum over all geodesic distances between any pair of points in the chosen sparse point set. We compute intersection configuration using 1-norm.

Correspondence search: Finally, for every pair of meshes in the same object class, we consider combinations of point correspondence sets and evaluate the ICD error measure for each one. We log the ICD computed for correspondence sets that are both correct and incorrect and then gather statistics to analyze how well the ICD is able to discriminate between
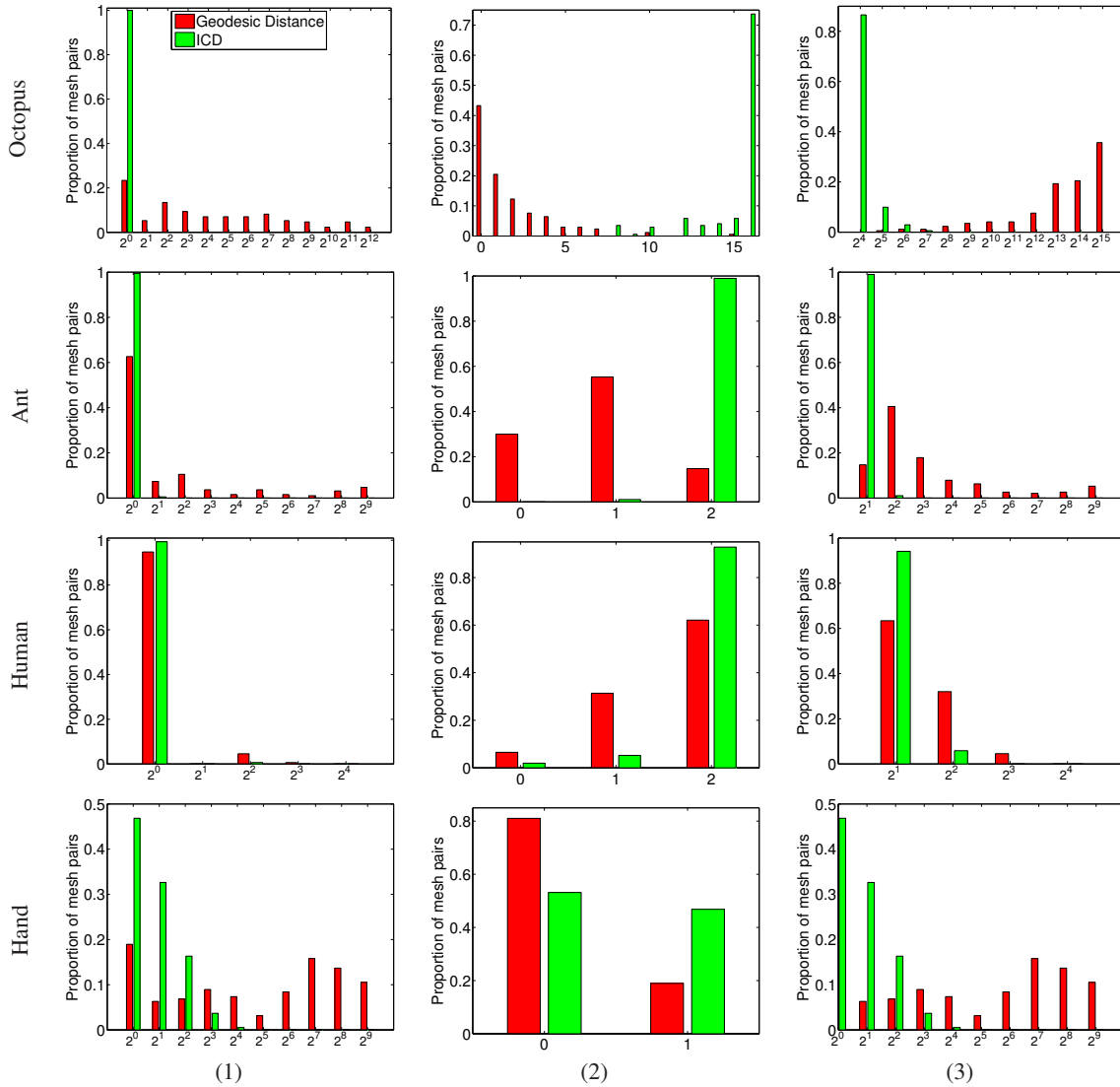
Figure 5: *intersection configuration distance vs. consistency of pairwise geodesic distance. The histograms of the following three statistics over all pairs within the same category: **(1)**: when the first correct permutation appears, **(2)**: the number of correct ones in the first k permutations where k is the the number of elements in the ground truth set, **(3)**: when all correct permutations are included.*
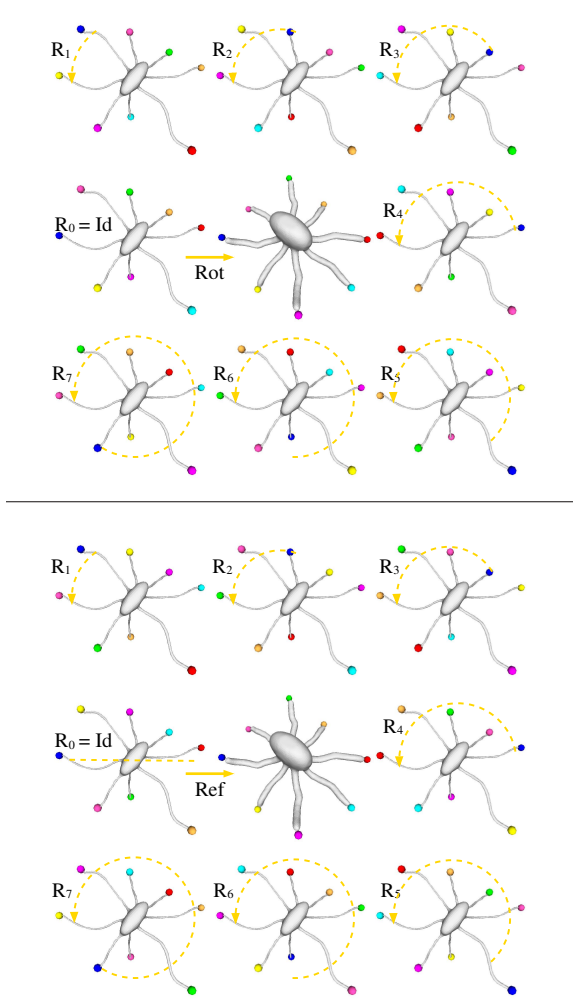
them. We compare our results to ones computed using differences of pairwise geodesic distances between corresponding feature points [BBK06].

Timing: Table 1 shows timing results collected on a PC with Core2 Duo CPU 2.40GHz and 4GB of memory. For most models tested, it takes around 10 seconds to detect a set of feature points (FP) and compute their intersection configuration (IC). Computing the distance between two intersection configurations is almost instantaneous.
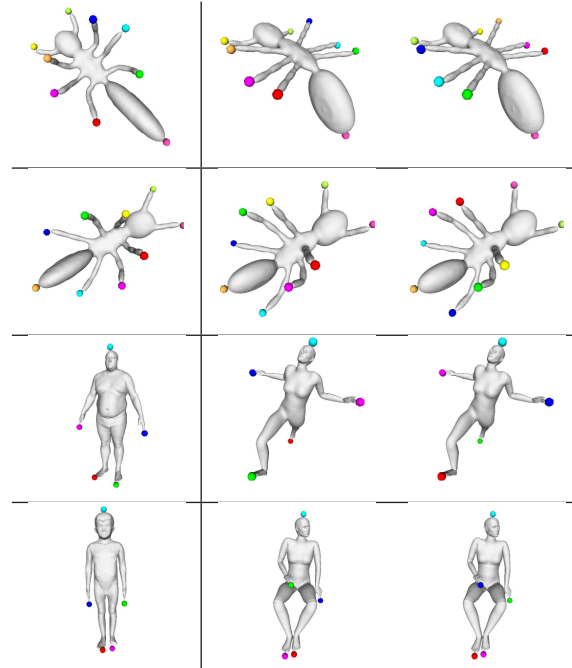
5.1. Permutation results

Our first experiment investigates the effectiveness of the ICD error measure when both the sparse point set $S = \{s_i\}_{i=1}^{m}$ and its image $h(S)$ are given but the exact map between them is unknown. There are totally $m!$ possible permutations between S and $h(S)$. We evaluate ICD for each permutation h and check whether it discriminates good maps from bad ones.

For this experiment, we limit the data set to the four categories for which our algorithm is able to extract point fea-

Figure 7: *The first two permutations for two pairs of humans and two pairs of ants.*

Figure 6: *The first 16 permutations of Octopus* 122 *and Octopus* 124 *based on ICD, which form a group similar to the dihedral group* D_8*. The top three rows show all rotations* $Rot \circ R_i$ *and the bottom three rows show all reflections* $Ref \circ R_i$*, where Rot preserves the orientation, Ref reverses the orientation, and* R_i*'s are self-rotation of Octopus* 122*.*

tures consistently for all meshes in the same category: Human, Ant, Octopus, and Hand. For each category, we establish a ground truth set of correspondences and test to see how well our methods recover them. Specifically, we sort all possible permutations in the increasing order of their error measure, and then search along this sorted list to see (1) when the first correct permutation appears, (2) the number of correct ones in the first k permutations where k is the the number of elements in the ground truth set, (3) when all correct permutations are included. The histograms of these three statistics for each category are shown in Figure 5, which shows the in-
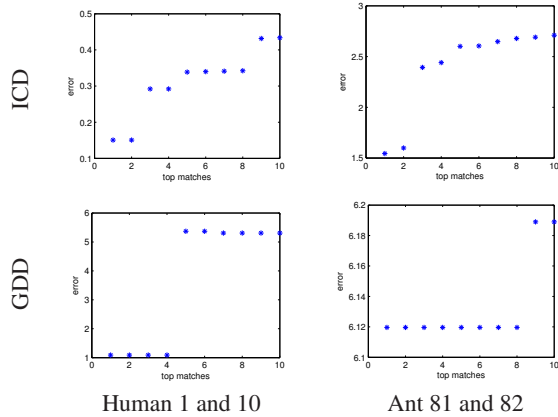
tersection configuration distance performs much better than the difference of pairwise geodesic distances.

For example, in the category of Octopus, each mesh has self intrinsic symmetry group similar to dihedral group D_8, which has 16 elements. For each octopus (except Octopus 125 which only has four arms), our point selection algorithm chooses 8 points on the tip of each arm. For each pair of octopi, we measure the error of each permutation either by its intersection configuration distance (green bars) or by the differences of pairwise geodesic distances (red bars). As we can see from Figure 5, the intersection configuration distance performs very well: the first permutation is always correct (1st column), and in more than 70% pairs, the first 16 permutations are all correct (2nd column). Figure 6 shows the first 16 permutations between a pair of octopi, which forms a group similar to D_8. In contrast, from Figure 5, the error measure based on the difference of pairwise geodesic distances performs poorly: in about 40% pairs, there is no correct permutations in the first 16 ones (2nd column) and one needs to retrieve about $2^{15} = 32,768$ permutations in order to find all 16 correct permutations (3rd column).

The statistics for the category of Human and Ant are also shown in Figure 5, which shows that the IDC performs very well: in almost all pairs of humans and ants, two correct permutations have the smallest intersection configuration distances. Note we exclude Human 16 and Human 18 as they are topologically different from the others. Figure 7 shows the first two permutations for two pairs of humans and two

Human 1 and 10   Ant 81 and 82

Figure 8: *ICD: the intersection configuration distances of the first* 10 *permutations of a pair of ants and a pair of humans; GDD: the differences of pairwise geodesic distances of the first* 10 *permutations of a pair of ants and a pair of humans. Note there are only two correct permutations for a pair of humans or ants.*

pairs of ants. One permutation maps the left to the left and the other maps the left to the right. From Figure 8, we can see there is a gap in the ICDs between two consistent permutations and others. In fact, similar phenomena are observed in almost all pairs of ants and all pairs of humans

For Human, it appears that the differences of pairwise geodesic distances perform also well. However, further examination shows that the differences of pairwise geodesic distances can hardly distinguish the two correct permutations from the following two: 1) switching the left hand with the right one but keeping the feet unchanged, i.e., mapping the left to the left foot and the right foot to the right, 2) switching the left foot with the right one but keeping the hands unchanged, see Figure 8. It is somehow a coincidence that in about 90% pairs, the permutation with the smallest difference of pairwise geodesic distances is correct (1st column). In fact, only in about 60% pairs, can the differences of pairwise geodesic distances pick out both correct permutations (3rd column).

For the hand category, ICD again performs much better than the differences of pairwise geodesics, see Figure 5. However, notice that there are more mispredictions in the category of hand than in other categories. Further examination shows that most of the top misprediction are like the map shown in the top right cell in Figure 9, which swaps thumb with little finger and index finger with ring finger, and in some sense is still spatially consistent. In fact, in about 80% pairs, the first two permutations contains the correct one (1st column and 3rd column in Figure 5). In Figure 9, its first column shows the first permutation for each of two pairs of hands, and its second column shows the first two permu-

(a)   (b)
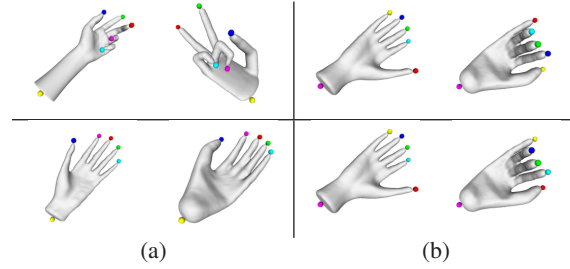
Figure 9: *Correspondences of hands. (a) the first permutation for each of two pairs of hands, (b) the first two permutations of a pair of hands.*

tations of a different pair. Although the first one (top) is not correct, it flips the hand in a consistent way as we explain above.

5.2. Subset search results

In this section, we consider a harder problem: given a sparse point set $S_X = \{x_i\}_{i=1}^m \in X$ and a point set $S_Y = \{y_i\}_{i=1}^{m'} \in Y$, assuming that $h(S_X)$ is contained in S_Y for each consistent correspondence $h : S_X \rightarrow Y$, find a consistent correspondence h. This problem is more general in the sense that we lose the assumption of $h(S_X) = S_Y$. Now, $h(S_X) \subset S_Y$, a more typical search scenario.

In this setting, although m is small, m' can be large which prevents us from searching all possible maps from S_X into S_Y. Thus, some heuristic search strategy has to be employed, such as branch-and-bound [GMGP05], priority-driven search [FS06], or belief propagation [ASP*04]. In the paper, we use a simple heuristic searching algorithm called beam search [Low76] mainly to show that even for a very sparse point set, its intersection configuration conveys enough geometric information to distinguish the good map from bad ones.

Beam search uses breadth-first search to build its search tree. Each node in the tree represents a map from a subset of S_X into S_Y. The tree starts with an empty root at level 0 and grows as follows. For each node at level i, generate m' successors each of which adds one more pair from x_{i+1} to one of points in S_Y. Update the ICD for the map represented by each successor of any node at level i. Sort them in the increasing order of their error measures and only keep part of them with small error measures as the nodes at level $(i+1)$. In our implementation, we do not perform pruning in the first few levels. If we start to prune, we only keep the first $1/m'$ of the total nodes on that level so that the number of nodes on the afterward levels remains fixed.

We apply beam search to the shapes in the category of Armadillo and Fourleg. Note that for each pair shown in the following figures, we map the left one into the right one,
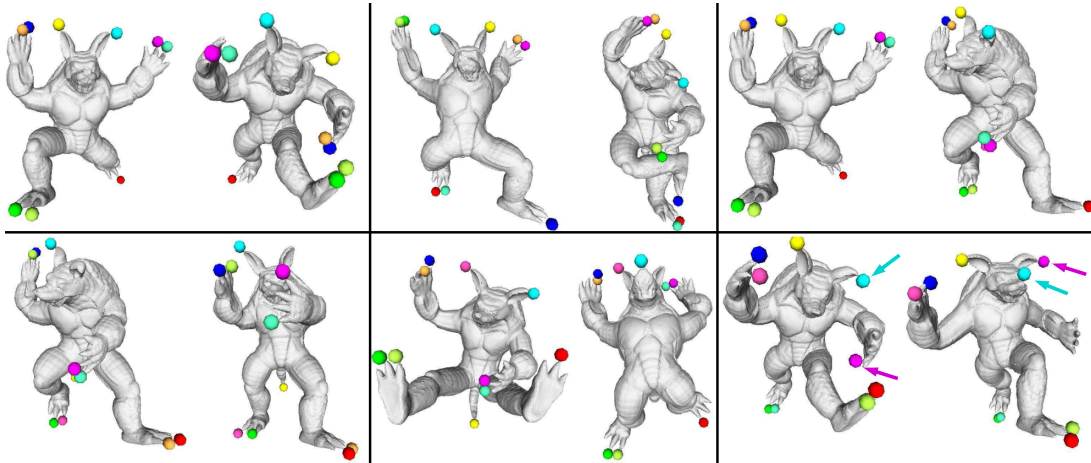
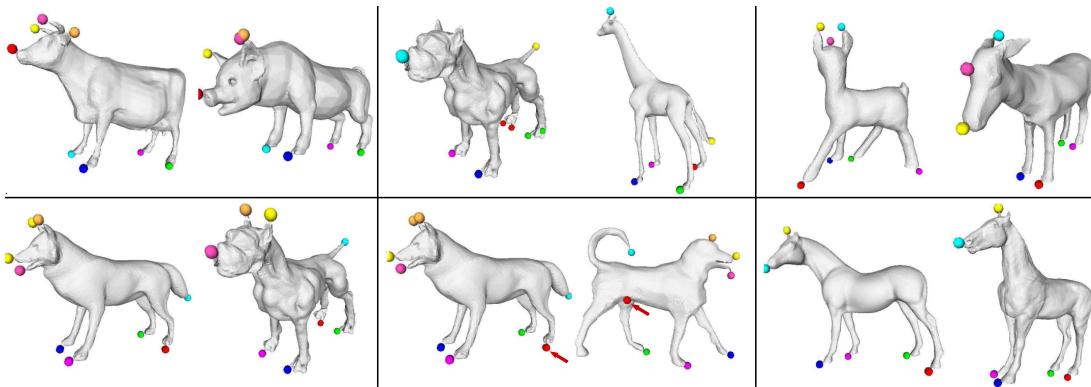**Figure 10:** *Correspondences for category armadillo*

Figure 11: *Correspondences for category fourleg*

meaning we choose less points from the left one than from the right one as stated in our problem. For Armadillo, we set $m = 10$ and $m' = 20$ and we start to prune at level 5. For Fourleg, we set $m = 8$ and $m' = 15$ and we start to prune at level 5. It is possible that some shapes do not have the prescribed number of maxima.

Figure 10 and Figure 11 show the correspondence of the smallest intersection configuration distance on the leaf level for a few pairs of armadillos and fourleg animals. As we can see, our intersection configuration distance can generally find a spatially consistent correspondence. However, there are some failure cases. For example, in the pair shown in the bottom rightmost cell in Figure 10, the point on the left hand (pink) maps to the left ear while the point on the left ear (cyan) maps to the tip to the nose. Also, in the pair shown in the bottom middle cell in Figure 11, a point on a leg (red) is mapped to the bottom of the body. Nevertheless, in the above two failed cases, further investigation shows that the correct correspondences also have small intersection configuration

distances. We believe that combining intersection configuration with some local point signature like HKS can resolve this ambiguity. However this is not the focus of the paper and we leave it as future work.

Finally, Figure 12 shows the correspondence of the smallest intersection configuration distance for a couple pairs of armadillos where some major parts of an armadillo are missing. When we map an armadillo with major parts missing into a complete one, as required by our assumption, the beam search can still find a reasonable correspondence.

6. Conclusion

In this paper, we have introduced a new concept, fuzzy geodesics, based on which we define the intersection configuration associated with a set of points on a manifold, which encodes the spatial relation between them. We demonstrate its effectiveness in the application of finding consistent correspondences between sparse sets of points on shapes differ-
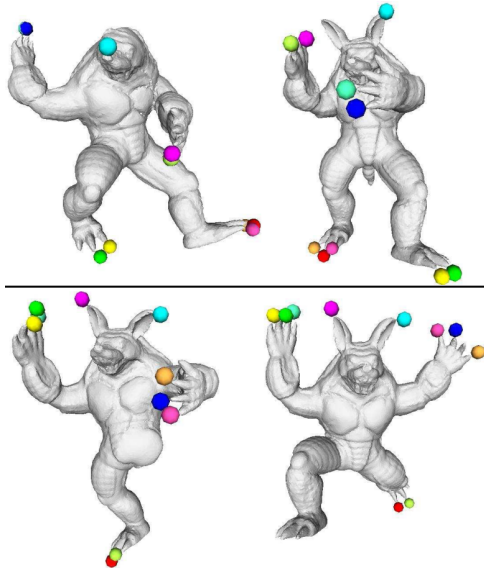
Figure 12: *Correspondences for two pairs of armadillos. The armadillos on the left side have some major parts missing.*

ing by extreme deformations. In the future, we would like to investigate other theoretical properties of fuzzy geodesics, as well as other applications.

References

[ASP*04] ANGUELOV D., SRINIVASAN P., PANG H., KOLLER D., THRUN S., DAVIS J.: The correlated correspondence algorithm for unsupervised registration of nonrigid surfaces. In *NIPS* (2004), vol. 17, pp. 33–40.

[ATCO*10] AU O. K.-C., TAI C.-L., COHEN-OR D., ZHENG Y., FU H.: Electors voting for fast automatic shape correspondence. In *Computer Graphics Forum (In Proc. of Eurographics 2010)* (2010), vol. 29, p. to appear.

[BBK06] BRONSTEIN A., BRONSTEIN M., KIMMEL R.: Generalized multidimensional scaling: A framework for isometry-invariant partial surface matching. *Proceedings of the National Academy of Science* (2006), 1168–1172.

[BR07] BROWN B. J., RUSINKIEWICZ S.: Global non-rigid alignment of 3-d scans. *ACM Trans. Graph. 26*, 3 (2007), 21.

[dC92] DO CARMO M. P.: *Riemannian Geometry*. Birkhäuser, Boston, MA, USA, 1992.

[DL09] DEY T. K., LI K.: Cut locus and topology from surface point data. In *SCG '09: Proceedings of the 25th annual symposium on Computational geometry* (New York, NY, USA, 2009), ACM, pp. 125–134.

[ELZ00] EDELSBRUNNER H., LETSCHER D., ZOMORODIAN A.: Topological persistence and simplification. In *FOCS '00: Proceedings of the 41st Annual Symposium on Foundations of Computer Science* (Washington, DC, USA, 2000), IEEE Computer Society, p. 454.

[FS06] FUNKHOUSER T., SHILANE P.: Partial matching of 3d

shapes with priority-driven search. In *Symposium on Geometry Processing* (2006).

[GBP07] GIORGI D., BIASOTTI S., PARABOSCHI L.: SHREC:SHape REtrieval Contest: Watertight models track, http://watertight.ge.imati.cnr.it/, 2007.

[GMGP05] GELFAND N., MITRA N. J., GUIBAS L. J., POTTMANN H.: Robust global registration. In *Symposium on Geometry Processing* (2005).

[Gro99] GROMOV M.: *Metric Structures for Riemannian and Non-Riemannian Spaces*. Birkhäuser, Boston, MA, USA, 1999.

[HPW06] HILDEBRANDT K., POLTHIER K., WARDETZKY M.: On the convergence of metric and geometric properties of polyhedral surfaces. *Geometriae Dedicata 123*, 1 (December 2006), 89–112.

[HSKK01] HILAGA M., SHINAGAWA Y., KOHMURA T., KUNII T. L.: Topology matching for fully automatic similarity estimation of 3D shapes. In *Proceedings of SIGGRAPH 2001* (August 2001), Computer Graphics Proceedings, Annual Conference Series, pp. 203–212.

[JZvK07] JAIN V., ZHANG H., VAN KAICK O.: Non-rigid spectral correspondence of triangle meshes. *International Journal on Shape Modeling 13*, 1 (2007), 101–124.

[LF09] LIPMAN Y., FUNKHOUSER T.: Mobius voting for surface correspondence. *ACM Transactions on Graphics (Proc. SIGGRAPH) 28*, 3 (August 2009).

[Low76] LOWERRE B. T.: *The harpy speech recognition system*. PhD thesis, Pittsburgh, PA, USA, 1976.

[MMP87] MITCHELL J. S. B., MOUNT D. M., PAPADIMITRIOU C. H.: The discrete geodesic problem. *SIAM J. Comput. 16*, 4 (1987), 647–668.

[MS05] MÉMOLI F., SAPIRO G.: A theoretical and computational framework for isometry invariant recognition of point cloud data. *Found. Comput. Math. 5*, 3 (2005), 313–347.

[OSG08] OVSJANIKOV M., SUN J., GUIBAS L.: Global intrinsic symmetries of shapes. *Computer Graphics Forum (Symposium on Geometry Processing) 27*, 5 (2008), 1341–1348.

[Pap85] PAPADIMITRIOU C.: An algorithm for shortest-path motion in three dimensions. *IPL 20* (1985), 259–163.

[SMC07] SINGH G., MEMOLI F., CARLSSON G.: Topological Methods for the Analysis of High Dimensional Data Sets and 3D Object Recognition. Botsch M., Pajarola R., Chen B., Zwicker M., (Eds.), Eurographics Association, pp. 91–100.

[SOG09] SUN J., OVSJANIKOV M., GUIBAS L. J.: A concise and provably informative multi-scale signature based on heat diffusion. *Comput. Graph. Forum 28*, 5 (2009), 1383–1392.

[SSK*05] SURAZHSKY V., SURAZHSKY T., KIRSANOV D., GORTLER S. J., HOPPE H.: Fast exact and approximate geodesics on meshes. *ACM Trans. Graph. 24*, 3 (2005), 553–560.

[vKZHCO10] VAN KAICK O., ZHANG H., HAMARNEH G., COHEN-OR D.: A survey on shape correspondence. In *EUROGRAPHICS STAR Report* (2010).

[WGQ08] WANG S., GU X., QIN H.: Automatic non-rigid registration of 3d dynamic data for facial expression synthesis and transfer. In *Proceedings of the IEEE Computer Vision Pattern Recognition 2008 (CVPR08)* (Anchorage, Alaska, USA, June 2008).

[ZSCO*08] ZHANG H., SHEFFER A., COHEN-OR D., ZHOU Q., VAN KAICK O., TAGLIASACCHI A.: Deformation-driven shape correspondence. *Comput. Graph. Forum 27*, 5 (2008), 1431–1439.